

Deoxyhypusine hydroxylase: A novel therapeutic target differentially expressed in short-term vs long-term survivors of glioblastoma

Paula Ofek¹  | Eilam Yeini¹  | Gali Arad² | Artem Danilevsky^{3,4} |
 Sabina Pozzi¹ | Christian Burgos Luna¹ | Sahar Israeli Dangoor¹ |
 Rachel Grossman⁵ | Zvi Ram⁵ | Noam Shomron^{3,4,6} | Henry Brem⁷ |
 Thomas M. Hyde^{8,9,10} | Tamar Geiger² | Ronit Satchi-Fainaro^{1,6}  

¹Department of Physiology and Pharmacology,
 Sackler Faculty of Medicine, Tel Aviv
 University, Tel Aviv, Israel

²Department of Molecular Genetics, Sackler
 Faculty of Medicine, Tel Aviv University, Tel
 Aviv, Israel

³Department of Cell and Developmental
 Biology, Sackler Faculty of Medicine, Tel Aviv
 University, Tel Aviv, Israel

⁴Edmond J Safra Center for Bioinformatics,
 Tel Aviv University, Tel Aviv, Israel

⁵Department of Neurosurgery, Tel Aviv
 Sourasky Medical Center, Tel Aviv, Israel

⁶Sagol School of Neurosciences, Tel Aviv
 University, Tel Aviv, Israel

⁷Department of Neurosurgery, Johns Hopkins
 University School of Medicine, Baltimore,
 Maryland, USA

⁸Lieber Institute for Brain Development, Johns
 Hopkins Medical Campus, Baltimore,
 Maryland, USA

⁹Department of Psychiatry & Behavioral
 Science, Johns Hopkins University School of
 Medicine, Baltimore, Maryland, USA

Abstract

Glioblastoma (GB) is the most aggressive neoplasm of the brain. Poor prognosis is mainly attributed to tumor heterogeneity, invasiveness and drug resistance. Only a small fraction of GB patients survives longer than 24 months from the time of diagnosis (ie, long-term survivors [LTS]). In our study, we aimed to identify molecular markers associated with favorable GB prognosis as a basis to develop therapeutic applications to improve patients' outcome. We have recently assembled a proteogenomic dataset of 87 GB clinical samples of varying survival rates. Following RNA-seq and mass spectrometry (MS)-based proteomics analysis, we identified several differentially expressed genes and proteins, including some known cancer-related pathways and some less established that showed higher expression in short-term (<6 months) survivors (STS) compared to LTS. One such target found was deoxyhypusine hydroxylase (DOHH), which is known to be involved in the biosynthesis of hypusine, an unusual amino acid essential for the function of the eukaryotic translation initiation factor 5A (eIF5A), which promotes tumor growth. We consequently validated DOHH overexpression in STS samples by quantitative polymerase chain reaction (qPCR) and immunohistochemistry. We further showed robust inhibition of

Abbreviations: ATP, adenosine triphosphate; CD31, cluster of differentiation 31; CDK, cyclin-dependent kinase; CEP170B, centrosomal protein 170B; CHI3L1, chitinase 3 like 1; CPX, cyclopirox; DAPI, 4',6-diamidino-2-phenylindole; DEF, deferiprone; DHPS, deoxyhypusine synthase; DMEM, Dulbecco's Modified Eagle Medium; DOHH, deoxyhypusine hydroxylase; ECACC, European Collection of Authenticated Cell Cultures; EGFR, epithelial growth factor receptor; eIF5A, eukaryotic translation initiation factor 5A; EMP3, epithelial membrane protein 3; EMT, epithelial-mesenchymal transition; FBLN4, fibulin-4; FBS, fetal bovine serum; FDR, false discovery rate; FFPE, formalin-fixed paraffin-embedded; GAPDH, glyceraldehyde-3-phosphate dehydrogenase; GFR, growth factors reduced; GLUT1, glucose transporter 1; HIF-1 α , hypoxia-inducible factor 1-alpha; HRP, horseradish peroxidase; IDH1/2, isocitrate dehydrogenase 1/2; IGFBP2/3, insulin-like growth factor binding protein-2/3; ILK, integrin-linked kinase; iRFP, near-infrared fluorescent protein; Ki-67, marker of proliferation Ki-67; KPS, Karnofsky performance status; LC-MS, liquid chromatography mass spectrometry; LGALS3, galectin 3; LTS, long-term survivors; MAOB, monoamine oxidase B; MAPK, mitogen-activated protein kinase; MGMT, O-6-methylguanine-DNA methyltransferase; mTOR, mammalian target of rapamycin; NF- κ B, nuclear factor kappa-light-chain-enhancer of activated B cells; NGS, next-generation sequencing; NRAS, NRAS proto-oncogene, GTPase; OCT, optimal cutting temperature compound; PARVA, Parvin alpha; PBS, phosphate saline buffer; PD-GB, patient-derived glioblastoma; PDK1, phosphoinositide-dependent kinase-1; PDPN, podoplanin; PFA, paraformaldehyde; PGK1, phosphoglycerate kinase 1; PI3K, phosphoinositide 3-kinase; PSN, penicillin, streptomycin and nystatin; qPCR, quantitative polymerase chain reaction; RBC, red blood cells; RHOA, Ras homolog family member A; ROS, reactive oxygen species; RR, ribonucleotide reductase; SCMIC, Sackler Cellular and Molecular Imaging Center; shRNA, short hairpin RNA; STS, short-term survivors; TASMC, Tel Aviv Sourasky Medical Center; TCA, tricarboxylic acid; TCGA, The Cancer Genome Atlas; TIMP1, TIMP metallopeptidase inhibitor 1; VEGF, vascular endothelial growth factor.

This is an open access article under the terms of the [Creative Commons Attribution-NonCommercial-NoDerivs](#) License, which permits use and distribution in any medium, provided the original work is properly cited, the use is non-commercial and no modifications or adaptations are made.

© 2023 The Authors. *International Journal of Cancer* published by John Wiley & Sons Ltd on behalf of UICC.

¹⁰Department of Neurology, Johns Hopkins University School of Medicine, Baltimore, Maryland, USA

Correspondence

Ronit Satchi-Fainaro, Department of Physiology and Pharmacology, Sackler Faculty of Medicine, Tel Aviv University, Ramat Aviv, Tel Aviv 69978, Israel.

Email: ronitsf@tauex.tau.ac.il

Funding information

H2020 European Research Council, Grant/Award Numbers: 835227, 862580; Israel Cancer Research Fund, Grant/Award Number: ICRF-PROF-18-682; Israel Science Foundation, Grant/Award Number: 1969/18; Morris Kahn Foundation

proliferation, migration and invasion of GB cells following silencing of DOHH with short hairpin RNA (shRNA) or inhibition of its activity with small molecules, ciclopirox and deferiprone. Moreover, DOHH silencing led to significant inhibition of tumor progression and prolonged survival in GB mouse models. Searching for a potential mechanism by which DOHH promotes tumor aggressiveness, we found that it supports the transition of GB cells to a more invasive phenotype via epithelial-mesenchymal transition (EMT)-related pathways.

KEY WORDS

deoxyhypusine hydroxylase (DOHH), glioblastoma, long-term survivors, proteogenomics, short-term survivors

What's new?

Despite surgical removal, tumor recurrence in glioblastoma is common. Recurrence is compounded by the heterogenous and drug-resistant nature of glioblastoma, which limits therapeutic options. Here, using RNA-seq and mass spectrometry-based proteomics analysis, the authors investigated candidate markers for associations with favorable prognosis in samples from glioblastoma patients with differing survival rates. Analyses reveal genes and proteins with differential expression, among them deoxyhypusine hydroxylase (DOHH), which is overexpressed in short-term survivors. DOHH, which catalyzes the final step in hypusine biosynthesis, an amino acid involved in promoting tumor growth, is a promising target for therapeutically diminishing glioblastoma progression and aggressiveness.

1 | INTRODUCTION

Glioblastoma (GB) is the most aggressive primary brain tumor in adults. The standard of care consists of surgery followed by adjuvant chemoradiotherapy. Due to the infiltrative nature of GB, tumor recurrence following surgical removal is common. Heterogeneity and high resistance of GB lead to limited therapeutic options. Only a modest impact on the overall survival of GB patients was achieved in the last few decades, with only 5% of GB patients reaching a 5-year survival.¹

In the last decade, several high-throughput genomics and proteomics studies have intended to establish clinically relevant GB subtypes. Patient basic attributes previously associated with long-term survival include younger age, higher Karnofsky score, gross total resection and increased immunity.² Genetic markers coupled with long-term survival include Isocitrate Dehydrogenase 1/2 (IDH1/2) gene mutations,³ O-6-Methylguanine-DNA methyltransferase (MGMT) promoter methylation, decreased expression of the chitinase 3 like 1 (CHI3L1), fibulin-4 (FBLN4), epithelial membrane protein 3 (EMP3), insulin-like growth factor binding protein-2/3 (IGFBP2, IGFBP3), galectin 3 (LGALS3), monoamine oxidase B (MAOB), podoplanin (PDPN), TIMP metallopeptidase inhibitor 1 (TIMP1), epithelial growth factor receptor (EGFR) and others.⁴ GB has been widely characterized and thoroughly analyzed at the genomic, transcriptional and histopathological levels in numerous cell lines, animal models and patient samples.^{5,6} Molecular characterization has provided a better understanding of GB biology; however, isolating the key genes and proteins that regulate the cellular processes that determine a tumor's

aggressiveness is yet a hurdle. We hypothesized that a comprehensive examination of the group of patients that survive longer (referred to from now on as long-term survivors [LTS]) vs short-term survivors (STS) might shed some light on the molecular pathways that mediate GB aggressiveness. For that purpose, we assembled a proteogenomic dataset of 87 GB clinical samples of varying survival rates. We performed RNA-seq and MS-based proteomics analysis to identify differentially expressed genes and proteins that regulate molecular mechanisms that determine prognosis.⁷ A direct comparison between STS and LTS tumors pointed at the increased activity of several well-known cancer signaling pathways such as mitogen-activated protein kinase (MAPK), phosphoinositide 3-kinase (PI3K), mammalian target of rapamycin (mTOR), NRAS proto-oncogene, GTPase (NRAS) and Ras Homolog family member A (RHOA) in STS patient samples. Moreover, we found differential expression of additional targets whose role in GB progression is less established, such as deoxyhypusine hydroxylase (DOHH).

DOHH catalyzes the activation of a unique family of cellular proteins, among them the eukaryotic translation initiation factor 5A (eIF5A), which is essential for cell growth and proliferation. Hypusine (N-4-amino-2-hydroxybutyl[lysine]) is a natural amino acid formed by conjugating the aminobutyl moiety of the polyamine spermidine to a specific lysine residue of eIF5A. Hypusine is vital for eIF5A activity, and its synthesis is catalyzed by deoxyhypusine synthase (DHPS) and DOHH. The long sidechain of hypusine promotes eIF5A-mediated translation, elongation and termination by enhancing peptide bond formation and peptide release. eIF5A, DHPS and DOHH are highly conserved in all eukaryotes, and so is the

hypusine site, suggesting the critical role of this pathway.^{8,9} Increased levels of eIF5A were reported in several cancer types, including GB.¹⁰ However, the direct involvement of DOHH in GB was not reported before. Nevertheless, inhibitors of DHS and DOHH were developed and shown to hinder the proliferation of mammalian cells.^{11,12} Inactivation of both alleles of DOHH in a conditional knockout mouse model resulted in embryonic lethality, while a cell line derived from this mouse showed reduced proliferation and transformation potential.¹³ In addition, inhibition of DOHH using small molecules, such as ciclopirox (CPX) and deferiprone (DEF), led to a remarkable reduction in the proliferation of several cancer cell lines^{14–18} and decreased breast cancer and myeloma growth in mouse models.^{16,19} CPX is a well-known antifungal drug and has been in use for almost three decades.²⁰ As an iron chelator, it interferes with several key signaling pathways. Besides inhibiting DOHH/eIF5A, it modulates the activity of ribonucleotide reductase (RR), Wnt/β-catenin, hypoxia-inducible factor 1-alpha (HIF-1 α), vascular endothelial growth factor (VEGF), mTOR and cyclin-dependent kinases (CDKs). Another iron chelator, DEF (Ferriprox), is used to treat thalassemia major.⁸ Once it reaches the intracellular sites of iron accumulation, like the mitochondria, it impairs the activity of aconitase, which catalyzes the isomerization of citrate to isocitrate in the tricarboxylic acid (TCA) cycle.²¹ DEF also inhibits the mitochondrial complexes I and II, which are crucial for adenosine triphosphate (ATP) production and regulates the generation of reactive oxygen species (ROS) that causes cellular toxicity. These findings highlight the potential of these drugs to hinder cancer progression by several mechanisms, including DOHH inhibition.²²

In addition, miR-331-3p, shown to reduce DOHH-mRNA levels and inhibit prostate cancer cell proliferation²³ is downregulated in several GB cell lines, enhancing their growth potential.⁹ However, there is no direct evidence for the role of DOHH in GB tumorigenesis, or the feasibility of DOHH inhibitors to inhibit GB progression.

Hence, we aim to evaluate the role of DOHH in determining the aggressiveness of GB. In the current study, we uncover the therapeutic potential of mimicking the lower DOHH expression levels detected in long-term survivors. Following gene silencing or pharmacological inhibition of DOHH, we show a reduction in proliferation, migration and invasion of murine and human GB cells derived from cell lines or freshly isolated cells from patient-derived glioblastoma (PD-GB) samples. The effect of DOHH silencing was further evaluated in an orthotopic mouse model of GB, achieving a considerable inhibition in tumor progression and prolonging the overall survival. We lastly propose that DOHH exerts its tumorigenic effect by pushing GB cells toward a more invasive and aggressive phenotype.

2 | MATERIALS AND METHODS

2.1 | Materials

Dulbecco's Modified Eagle Medium (DMEM), Fetal Bovine Serum (FBS), L-glutamine, Penicillin, Streptomycin and Nystatin (PSN) solution, and EZ-RNA II total RNA isolation kit were purchased from Biological Industries Ltd (Beit HaEmek, Israel). Chemical reagents,

including ciclopirox and deferiprone, were purchased from Sigma-Aldrich (Rehovot, Israel). DNase I and Collagenase IV were from Worthington (NJ). qScript cDNA Synthesis Kit and PerFecTa SYBR Green FastMix ROX were from Quanta BioSciences (Beverly, MA).

2.1.1 | Human GB specimens

We obtained a total of 84 fresh frozen samples and 60 FFPE samples from Tel Aviv Sourasky Medical Center (TASMC). For 60 patients, we had both fresh frozen and FFPE samples (36 samples of STS [Survival 3.7 ± 0.2 months] and 24 samples of LTS [Survival 48 ± 3.9 months]), while for the additional 24 patients, we obtained only fresh frozen specimens. Human healthy brain FFPE samples were obtained from the Lieber Institute (Baltimore, MD).

2.2 | Mass spectrometry (LC-MS) analysis

Protein extraction from FFPE GB samples was performed as previously described.⁷ Cellular-rich areas were macro-dissected from tissue slices by overlaying H&E staining to exclude stromal components.

2.2.1 | RNA isolation

Total RNA isolation kit (EZ-RNA II, Biological Industries Ltd, Israel) was used according to the manufacturer's protocol.

2.2.2 | RNA-sequencing

RNA was isolated from 84 fresh frozen samples, and following quality control, sent to next-generation sequencing (NGS) analysis (HiSeq 2500, 20 million reads) (Otogenetics, Atlanta). The resulting reads in FASTQ format were trimmed and quality filtered. STAR aligner was used for sequence alignment and htseq count²⁴ for transcriptome expression quantification compared to Ensembl.

2.2.3 | Real-time PCR

The cDNA synthesis was performed using qScript cDNA synthesis (Quanta BioSciences) according to the manufacturer's protocol. The expression level of selected target genes was assessed by SYBR green real-time PCR (PerFecTa FastMix ROX, Quanta BioSciences) and normalized GAPDH expression level.

2.3 | Primers

DOHH: forward 5'-TCCTTGAGAGCGTTCACTATG-3', reverse 5'-CT GTCCACTGTCCAAGTTATC-3'

DOHH: forward 5'-GACTTTGAGCTACTGGGATCTG-3', reverse 5'-CAGGAAGTG ATGTTATGCCCTTG-3'
 VEGF: forward 5'-TGCCCGCTGCTGTCTAAT-3', reverse 5'-TCTCCGCTCTGAGCAAGG-3'
 PDK1: forward 5'-ACCAGGACAGCCAATACAAG-3', reverse 5'-CCTCGGTCACTCATCTTCAC-3'
 PGK1: forward 5'-CAGCTGCTGCTGGGTCTGTCAT-3', reverse 5'-GCTGGCTCGGCTTAACC-3'
 GLUT1: forward 5'-GGTTGTGCCATACTCATGACC-3', reverse 5'-CAGATAGGACATCCAGGGTAGC-3'
 GAPDH: forward 5'-ATTCCACCCATGGCAAATTC-3', reverse 5'-GGATCTCGCTCCTGGAAGATG-3'

2.3.1 | Plasmids

Lentiviral DOHH small hairpin RNA (shRNA) plasmids (V3SH11243, three sequences for human; V3SM11244, three sequences for murine) and one Negative Control shRNA (VSC11721) were purchased from GE Healthcare Dharmacon, Inc. (Colorado). pLVX-near-infrared fluorescent protein (iRFP) was used as previously described.²⁵

2.3.2 | Cell culture

Human U-251 MG (RRID:CVCL_0021) GB cells were from the European Collection of Authenticated Cell Cultures (ECACC), and murine GL261 (RRID:CVCL_Y003) GB cells were from the NCI (Frederick, MD). Cells were cultured in DMEM with L-glutamine, PSN and 10% FBS, at 37°C in 5% CO₂. All experiments were performed with mycoplasma-free cells at passages 5 to 10. All human cell lines have been authenticated using STR profiling within the last 3 years.

2.3.3 | Hypoxia conditions

Human U-251 MG GB cells were incubated in a Hypoxia Incubator Chamber (27310, Stem-Cell Technologies) at 37°C, overnight, according to the manufacturer's instructions.

Patient-derived GB cells (PD-GB) were isolated from human fresh biopsies obtained from TASMC, minced and incubated in DMEM with collagenase IV (160 U/mg) and DNase (125 U) for 2 to 3 h at 37°C, then pipetted through a cell strainer. Following red blood cells (RBC) lysis, pelleted cells were re-suspended in growing medium and seeded in culture dishes.

2.3.4 | Lentiviral infections

HEK293T (RRID:CVCL_0063) cells were transfected with DOHH-shRNA (DOHH-SH), negative control shRNA (NC-SH) (Dharmacon) or pLVX-iRFP together with psPAX2 (Addgene #12260)

and pCMV-VSV-G (Addgene #8454). Media-containing viruses were collected 48 hours following transfection. For infection, GB cells were incubated with viruses and 8 µg/mL polybrene (Hexadimethrine Bromide, Sigma Aldrich, Israel) for 8 to 16 hours. Following 48 hours, positive cells were selected by puromycin resistance for DOHH-SH and NC-SH lentiviral particles infection, and hygromycin for iRFP infection.

2.3.5 | Proliferation assay

Cells were seeded in 96-well plates. Twenty-four hours later, the medium was replaced with different concentrations of CPX or DEF. Cell viability was measured for 72 hours by the IncuCyte Zoom Live cell analysis system (Essen Bioscience). For CPX and DEF, IC₅₀ values were calculated by GraphPad Prism using nonlinear regression dose-inhibition statistical analysis (<https://www.graphpad.com/support/faq/how-to-determine-an-icsub50sub/>).

2.3.6 | Transwell migration and invasion assay

iRFP-labeled GL261, U-251 MG or PD-GB4 cells (1×10^5 cells/well) were seeded on top of a filter membrane in a Transwell insert (Costar, 8 µm). Cells were suspended in 100 µL DMEM without serum for migration; or in GFR Matrigel for invasion. Two to four hours later, inserts were transferred to 24-well plates. Serum-free medium (\pm CPX 20 µM) was added on top of the cell monolayer, whereas DMEM +10% FBS (positive control) or serum-free DMEM (negative control) was added to the lower chamber of the Transwell insert. Cells were allowed to migrate for 24 hours (migration) or 72 hours (invasion) before fixation. Migrated cells were fixed and imaged using the EVOS FL Auto cell imaging system (ThermoFisher Scientific). Results were analyzed by ImageJ software.

2.3.7 | Sprouting assay

Tumor spheroids were prepared from iRFP-labeled, PD-GB, human U-251 MG or murine GL261 GB cells using our modified hanging-drop method, as previously described.²⁶ GB spheroids were embedded in Growth factors reduced (GFR) Matrigel (BD Biosciences), seeded in a 96-well plate and incubated in growing medium with or without CPX (20 µM). The 3D spheroid invasion was visualized after 48 to 72 hours with an EVOS FL Auto cell imaging system (ThermoFisher Scientific, USA).

2.3.8 | Western blot

U-251 MG cells were lysed in RIPA buffer with protease and phosphatase inhibitors (Cell Signaling, MA). Protein concentration was assessed using a BCA protein assay (Pierce). Following SDS-PAGE,

proteins were incubated with anti-E-cadherin (24E10), and N-cadherin (D4R1H), (Cell Signaling, USA) or anti-human/murine DOHH antibody (sc-271 868, Santa Cruz Biotechnology). GAPDH and beta-actin were used for loading control (Ab9485 and Ab8226, respectively, Abcam). All primary antibodies were followed by HRP-conjugated secondary antibodies (Jackson ImmunoResearch) and SuperSignal West Pico Plus chemiluminescent substrate (Thermo Scientific). Images were developed using the iBright 1500 instrument (Life Technologies, USA).

2.3.9 | Animal experiments

Six-week-old male SCID mice (Envigo CRS, Israel) were anesthetized by intraperitoneal injection of ketamine and xylazine (150 and 12 mg/kg, respectively). U-251 MG (5×10^4 cells in 5 μ L), wild-type, DOHH-SH or NC-SH, were stereotactically implanted into the striatum of the mice ($n = 10$). Tumor volume was followed by MRI (MR solutions), and body weight was measured every other day. On day 29 post cell inoculation, $n = 3$ mice per group were euthanized, and brains were harvested for immunohistochemistry analysis. $n = 7$ mice per group were followed for survival.

2.3.10 | MRI imaging

Mice were injected intraperitoneally with 70 μ L contrast agent (Magnetol, Gd-DTPA, Soreq M.R.C. Israel Radiopharmaceuticals). T1 with contrast agent and T2 weighted images were taken by 4.7 T MRI-MRS 4000 (MR solutions) at the Sackler Cellular and Molecular Imaging Center (SCMIC).

2.3.11 | Frozen tissue fixation

Anesthetized mice were perfused with phosphate saline buffer (PBS), followed by 4% paraformaldehyde (PFA). Brains were incubated with 4% PFA for 4 hours, followed by 0.5 M sucrose for 1 hours and 1 M sucrose overnight. Tissues were then embedded in optimal cutting temperature compound (OCT) (Scigen) and stored at -80°C .

2.3.12 | Immunostaining

OCT-embedded samples were cut into 5- μm thick sections. Staining was performed using BOND RX autostainer (Leica) with the following antibodies: anti-human/mouse DOHH (sc-271 868, Santa Cruz Biotechnology), anti-human DOHH (NBP1-91994, from Novus), anti-Ki67 (NB500-170, from Novus) anti-CD31 (550 272, from BD Biosciences), followed by Alexa Fluor-488/647 corresponding secondary antibodies (Ab150079, Ab150077 from Abcam; 112-545-068 from Jackson ImmunoResearch). ProLong Gold mounting with DAPI (Invitrogen, USA) was added before slides were covered with coverslips. Images were taken using the

EVOS FL Auto cell imaging system (ThermoFisher Scientific) and quantified by ImageJ software.

2.3.13 | Immunostaining antibodies

Rabbit anti-human DOHH (NBP1-91994, from Novus). Goat anti-rabbit Alexa Fluor 647 (Ab150079)/Alexa Fluor 488 (Ab150077) were from Abcam (Cambridge, UK). Goat anti-rat Alexa Fluor 488 (112-545-068) was from Jackson ImmunoResearch Laboratories, Inc (PA).

2.3.14 | Statistical analysis

Data are expressed as mean \pm SD for in vitro assays or \pm SEM for in vivo assays. Statistical significance was determined using an unpaired *t*-test. All statistical tests were two-sided. One-dimensional (1D) annotation enrichment was performed as described.²⁷ Statistical analysis of proteomic data was corrected for multiple hypotheses using permutations-based false discovery rate (FDR) of 0.1 for *t*-test and Benjamini-Hochberg FDR of 0.02 for the 1D enrichment test. For Kaplan-Meier survival curves, *P* values were determined using two-tailed *P* values from log-rank (Mantel-Cox) test. For in vivo tumor growth curves, *P* values were determined using one-way ANOVA, Dunn's test or Holm-Sidak's test.

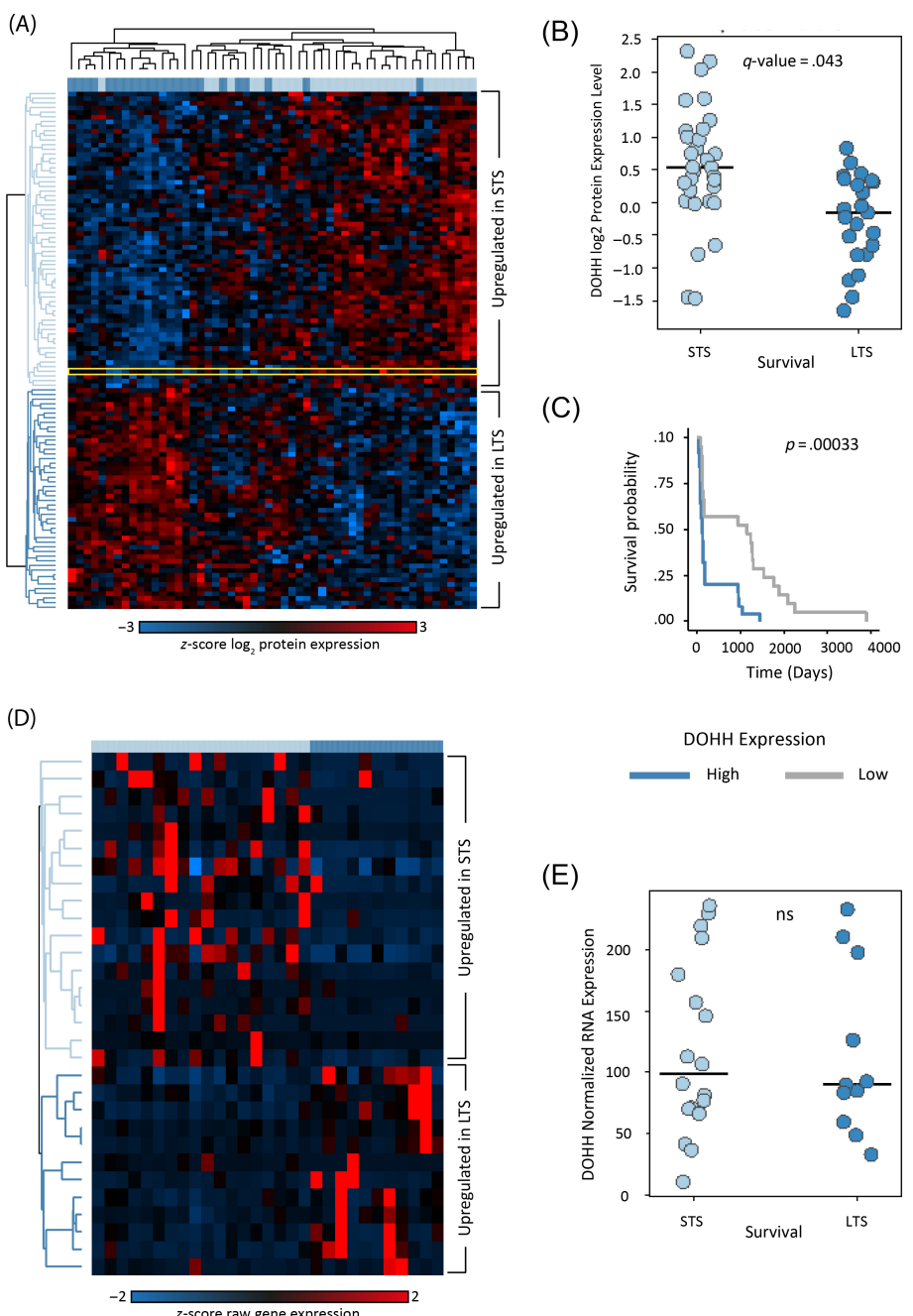
3 | RESULTS AND DISCUSSION

3.1 | DOHH is highly expressed in STS GB samples

We performed the analysis with 84 GB specimens, of which 54 had high-resolution proteomic data, 65 had high-quality RNA-seq data and 32 had both. To minimize sample variation, we focused on IDH1-wild type, untreated primary tumors.⁷ As expected, when analysis was performed, including IDH1-mutant samples, several RNA modules associated with survival showed a significant correlation to IDH1 status. Table S1 shows cohort details and patients' clinical information, including age and sex, which were very similar between the two groups. Sixty-nine samples were pathologically defined as primary GB; one sample was secondary GB. The cohort included tumors from 29 females, 49 males and 9 without sex information, with an age range of 19 to 85. Regression analysis found no significant association between these traits and survival except for the extent of tumor resection (*P*-value = .042). See Yanovich-Arad et al for a more detailed description of statistical analyses.⁷

Comparison of STS vs LTS proteomics data resulted in 112 differentially expressed proteins (*t*-test, FDR < 0.1), out of which 64 were upregulated in STS and 48 in LTS (Figure 1A, Table S2). As expected, we found an increased manifestation of several well-known cancer signaling pathways such as MAPK, PI3K-mTOR, NRAS and RHOA in STS tumors. We focused on targets whose role in GB progression is less established, such as Parvin Alpha (PARVA), Centrosomal Protein

FIGURE 1 Differential protein and gene expression in LTS vs STS GB human specimens. (A) Heatmap showing hierarchical clustering of 112 differentially expressed proteins (t -test, FDR < 0.1) out of which 64 are upregulated in STS samples (blue) and 48 are upregulated in LTS samples (dark red). Upper dendrogram and color bar represent sample separation. DOHH is highlighted in yellow. (B) Dot-plot showing the differential expression of DOHH in STS vs LTS GB samples (q -value = 0.043, FDR < 0.1). (C) Human GB patient samples were divided into two groups based on DOHH protein expression (Low = below median, High = above median). Kaplan-Meier analysis revealed a significant inverse correlation between DOHH expression and patients' survival (P -value = .00033). (D) Differential gene expression analysis was performed (using RNA-Seq) to compare STS vs LTS and is plotted in a heat map. (E) DOHH expression plotted vs survival (P -value = .967029).



170B (CEP170B) and DOHH. We are currently investigating PARVA and CEP170B; however, they are out of the scope of this article. DOHH, as mentioned above, catalyzes the activation of a unique family of cellular proteins, among them eIF5A, which is essential for cell growth and cell proliferation.²³

In this work, we focused on DOHH. We found that it is significantly upregulated in STS samples (Figure 1A, highlighted in yellow, Figure 1B). Using Kaplan-Meier analysis, we found DOHH protein expression to inversely correlate with patient survival (P = .00033, Figure 1C). The cutoff for DOHH expression was determined as the median, and patients were divided to either above or below it. Kaplan-Meier analysis was further validated using The Cancer

Genome Atlas (TCGA) RNA-seq dataset, showing a similar expression trend.⁷ Regarding the NGS analysis, the 40 most differentially expressed genes in the STS vs LTS samples are presented hereby, ordered by fold-change (Figure 1D, Table S3). We further show the normalized expression of DOHH plotted against survival (Figure 1E). Although the higher expression of DOHH in the STS group is nonsignificant according to the NGS data, there seems to be a trend in the same direction as shown in the proteomics which is supported in the following results.

The differences between the proteomics and NGS data regarding DOHH expression might be due to a complex gene regulation of DOHH. Given the key role DOHH might play in tumor cell

proliferation, we decided to further pursue experimentation on the gene, placing greater emphasis on the protein results at this point. Understanding how DOHH RNA is regulated, stored and released for downstream differential translation would be intriguing. This interesting topic is being investigated in follow-up studies.

Subsequently, we validated the results from the RNA-Seq and proteomics analyses by qPCR and immunohistochemistry, respectively (Figure 2). RNA isolated from GB fresh frozen samples was analyzed by qPCR, showing a significantly higher expression of DOHH in STS specimens compared to LTS (Figure 2A). The trend was similar to the NGS results, although those were nonsignificant. Of note, in an independent study that compared gene expression fold changes using RNA-Seq data from well-established reference samples, about 85% of the genes showed consistent results between RNA-Seq and qPCR data as these are based on different technologies.²⁸ In our case,

although some specimens yielded a very small amount of RNA, it was all used for RNA-Seq and there was no material left. Therefore, the qPCR analysis was performed only in 45 out of the 65 sequenced samples. This fact could have further contributed to the variability between both results.

Then, slides from STS and LTS FFPE samples were stained with anti-DOHH antibodies and DAPI to visualize the cell nuclei. We further evaluated normal brain samples. Immunostaining showed significantly higher DOHH expression in STS, lower levels in LTS and only minimal DOHH expression was found in healthy brain specimens (Figure 2B). We further evaluated murine GB samples compared to healthy brains and found notably higher DOHH expression levels in GB specimens (Figure 2C). These results confirm the proteogenomic findings and further support the role of DOHH in GB progression and aggressiveness.

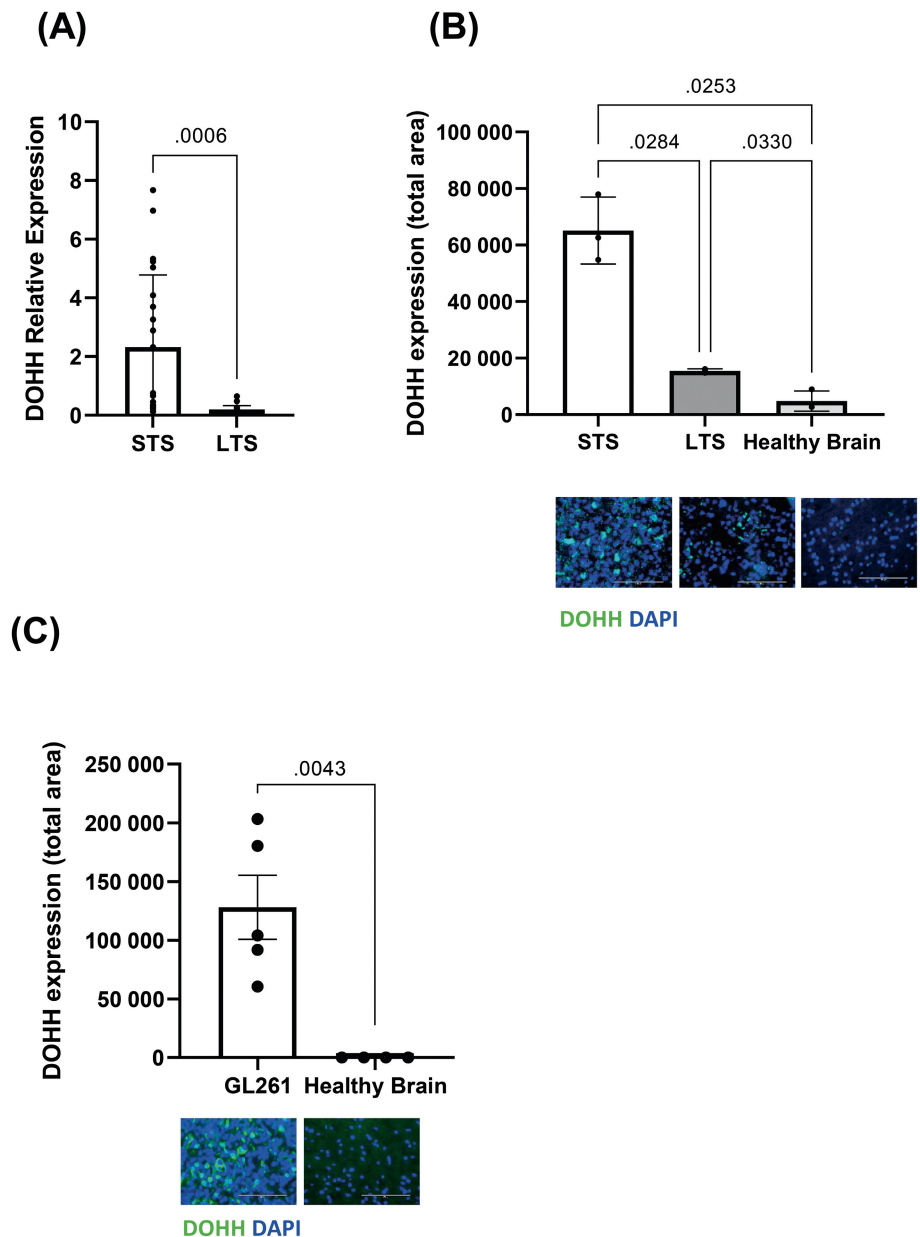


FIGURE 2 DOHH expression is higher in STS than in LTS GB samples, and higher in GB than healthy brain specimens. (A) Real-time PCR: RNA was isolated from fresh-frozen samples of GB human patients and analyzed by qPCR with specific primers for DOHH (STS $n = 23$, LTS $n = 22$). Bar plot shows the relative expression level of DOHH normalized to GAPDH. P -value = .0004. (B) Immunostaining: Representative images of FFPE samples from STS GB, LTS GB and normal brain human specimens, stained with anti-DOHH antibodies (green) and DAPI (blue = nucleus). Scale bar = 100 μ m. The total area stained with DOHH antibodies was quantified with ImageJ software. Data represent mean \pm SD ($n = 3$ tissue specimens per group, 4 images per sample). (C) Immunostaining: Representative images of OCT samples of GL261 intracranially injected GB tumor and healthy brain mouse specimens, stained with anti-DOHH antibodies (green) and DAPI (blue = nucleus). Scale bar = 100 μ m. The total area stained with DOHH antibodies was quantified with ImageJ software. Data represent mean \pm SD ($n = 3$ tissue specimens per group, 5 images for GL261 and 4 images for the healthy brain).

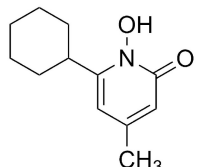
3.2 | DOHH inhibition or gene-silencing decreases the proliferation and migration of GB cells

To examine whether DOHH has a functional role in GB tumorigenicity, we used two well-established DOHH inhibitors: CPX and DEF (Figure 3A,B), which have been widely studied in culture and *in vivo*.²⁹ We assessed the proliferation rate of two GB cell lines: human U-251 MG, murine GL261 and two patient-derived primary GB cells (PD-GB3, PD-GB4) following treatment with CPX or DEF. The viability of all GB cells was notably reduced following DOHH inhibition, with an IC₅₀ of 0.9 to 1.7 µM for CPX and 32 to 78 µM for DEF (Figure 3C,D).

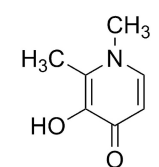
We further established GB cell lines stably expressing DOHH shRNA. We evaluated several Smart Vector Lentiviral DOHH shRNA

plasmids (3 human, 3 murine). Following infection with human DOHH shRNA2 (h-DOHH-SH2), human GB cells did not grow. Therefore, we evaluated two other sequences, as it was not possible to grow these cells in culture or perform any experiments with them. This might indicate the potential of inhibiting GB proliferation by completely knocking-out DOHH expression. While only 40% silencing was measured following infection with h-DOHH-SH3, cells infected with h-DOHH-SH1 showed an optimal silencing effect (close to 80%, Figure S1A) and we still managed to culture them. GL261 GB cells stopped proliferating following infection with murine DOHH shRNA3 (m-DOHH-SH3), while cells infected with m-DOHH-SH2 hardly showed any silencing, and m-DOHH-SH1 achieved the best possible DOHH knockdown (close to 70%, Figure S1B) that still enabled cell growth. Consequently, h-DOHH-SH1 and m-DOHH-SH1 were used

(A)



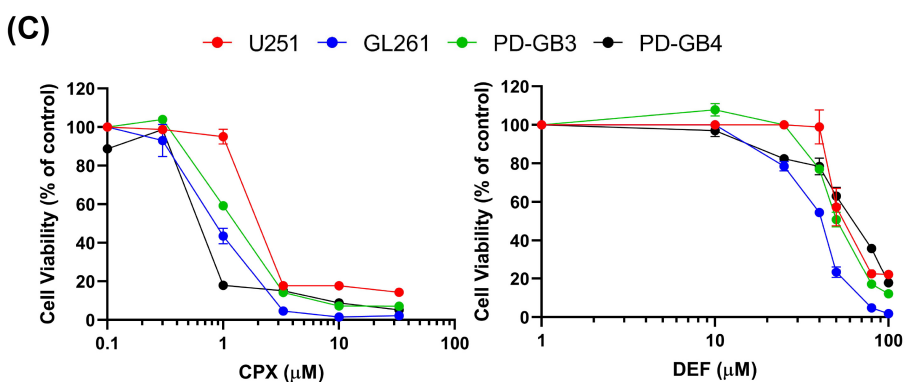
Ciclopirox



Deferiprone

(B)

	Full name	CAS Number	Empirical formula	Molecular Weight	PubChem ID
Ciclopirox (CPX)	Cyclohexyl-1-hydroxy-4-methyl-2(1H)-pyridone	41621-49-2	C ₁₂ H ₁₇ NO ₂ ⁻ C ₂ H ₇ NO	268.35	38911
Deferiprone (DEF)	Hydroxy-1,2-dimethyl-3-ethyl-4(1H)-pyridone	30652-11-0	C ₇ H ₉ NO ₂	139.15	2972



(D)

IC ₅₀ (µM)	U251	GL261	PD-GB3	PD-GB4
CPX	1.67	0.88	1.07	0.87
DEF	78.2	31.8	59.7	67.9

FIGURE 3 DOHH inhibition reduces proliferation of GB cells. (A) Chemical structures of the DOHH inhibitors, ciclopirox (CPX) and deferiprone (DEF). (B) Chemical properties of CPX and DEF. (C) Proliferation assay of human and murine GB cell lines (U-251 MG, GL261) and human patient-derived primary GB cells (PD-GB3, PD-GB4) with CPX and DEF. Data represent mean ± SD of triplicate wells. Each graph is representative of three independent repeats. (D) IC₅₀ values were calculated by nonlinear regression (GraphPad Prism) and are presented in a table.

for the following experiments with GB cells. DOHH knockdown was verified by qPCR (Figure S2A) and Western Blot (Figure S2B) displaying significant DOHH silencing.

Subsequently, a substantial decrease was observed in the viability of GL261 cells (Figure 4A), while the growth rate of U-251 MG cells (Figure 4A) was slightly inhibited following DOHH silencing. We then monitored the migration of U-251 MG and GL261 GB cells in a Transwell assay and found that DOHH silencing significantly inhibited the migration of both GB cells (Figure 4B). A similar effect of migration inhibition was observed following treatment with CPX (Figure 4B).

3.3 | Invasion and sprouting potential of GB cells is diminished following silencing or inhibition of DOHH

We assessed the invasion and sprouting ability of GB cells following DOHH knockdown in a Matrigel-TransWell assay and a 3D tumor-spheroid model (Figure 4C,D). DOHH silencing significantly inhibited the invasion of human GB cells compared to cells infected with negative control shRNA or untreated control cells. DOHH silencing by shRNA or pharmacological inhibition by CPX inhibited the growth and sprouting of 3D spheroids comprised of human GB cells (Figure 4C,D). We note that murine GL261 cells do not migrate through Matrigel, or form sprouting spheroids by this method and therefore were not included in those experiments. These findings point at a critical role of DOHH in the regulation of the adhesion and motility of GB cells, suggesting its involvement in EMT, as this process is linked to the invasion capabilities of various tumor cells including GB.³⁰

3.4 | DOHH knockdown inhibits tumor growth and prolongs survival in a human GB mouse model

We further evaluated the effect of DOHH inhibition *in vivo*, using a human GB mouse model. WT, DOHH-SH and NC-SH U-251 MG cells, previously established and characterized *in vitro*, were inoculated intracranially into SCID mice. Inhibition of tumor growth and prolonged survival were observed in the DOHH-SH group (Figure 5A,B). Of note, several attempts to use a negative control SH by two independent infections resulted in partial inhibition of tumor growth that was also significant. On day 29, three mice from each group were euthanized, and their brains were harvested and analyzed by immunostaining. These showed a lower microvessel density (CD31) and reduced proliferation (Ki-67) in DOHH-SH tumors (Figure 5C). Although microvessel density shows some inhibition in the NC-SH tumors (probably due to shRNA nonspecific effects), CD31 reduction is more remarkable in the DOHH-SH group.

Unfortunately, when we evaluated the effect of DOHH knockdown in the murine immunocompetent GL261 model, the results were disappointing (Figure S3). Preliminary *in vivo* experiments evaluating the therapeutic potential of CPX in the same GL261 murine GB

model were also unsuccessful (Figure S4). Nonetheless, oral-gavage CPX treatment has shown delayed tumor growth and prolonged mice survival in a GL261 subcutaneous tumor model (Figure S5). Although these results are not statistically significant, they may provide additional evidence of the need for a multitarget strategy, but also for the need to develop therapeutics that can reach the brain. Interestingly, evidence from the literature pointed to the possible role of DOHH pathway in immune-related functions while the different immune cells may react differently to DOHH inhibition.^{31,32} This may explain the different effects of DOHH inhibition between murine and PDX mouse models, as well as between the different tumor location. Further research investigating the specific role of this pathway in the brain tumor microenvironment is needed to fully understand these mechanisms. As we hypothesize that compensatory mechanisms could have affected the antitumor activity of DOHH inhibition, we are currently working on several therapeutic combination approaches; however, the results are still preliminary and out of the scope of this article. CPX itself in fact represents a multitarget approach, as it impacts multiple signaling pathways besides DOHH/eIF5A, such as ribonucleotide reductase, Myc, Wnt/β-catenin, VEGFR-3/ERK1/2 and ATR/Chk1/Cdc25A.³³ CPX prodrugs aiming to improve the bioavailability and solubility of CPX are currently being developed by several research groups.^{34,35} Moreover, several studies have indicated the therapeutic potential of targeting eif5a pathway in combination with additional therapeutic agents inhibiting other cellular and immune pathways such as imatinib,³⁶ ROS scavenger, N-acetyl-cysteine (NAC), TOP2A siRNA,³⁷ IFN α and DSH inhibitors.³⁸ These findings are directing us to alternative paths that probably will involve the combination of several targets.

3.5 | Proposed mechanism of DOHH anticancer effect on GB via regulation of EMT

Our results showing that DOHH silencing inhibits migration, invasion and sprouting of GB cells, point toward a potential connection between DOHH and EMT. Analysis of 163 samples from TCGA data using the GEPIA2 software,³⁹ led to a significant correlation between DOHH expression and EMT signature (including CDH2 [N-cadherin], ZEB1, ZEB2, CTNNB [Beta-catenin], TJP1 [ZO-1], VIM [vimentin], TWIST, Slug and Snail) in human GB samples (Figure 6A).

These findings support our hypothesis that EMT inhibition might be one of the mechanisms by which DOHH silencing decreases the invasion and sprouting of GB cells.

WT control, DOHH-SH and NC-SH U-251 MG GB cells were further analyzed by SDS-PAGE, and a remarkable E-cadherin upregulation together with N-cadherin downregulation was observed following DOHH silencing (Figure 6B). These data suggest a reasonable justification to the molecular mechanism by which DOHH higher expression correlates with GB-enhanced aggressiveness. An additional critical player in cancer progression that induces invasion, mesenchymal differentiation and radiation resistance in GB is nuclear factor kappa-light-chain-enhancer of activated B cells (NF-κB).^{40,41}

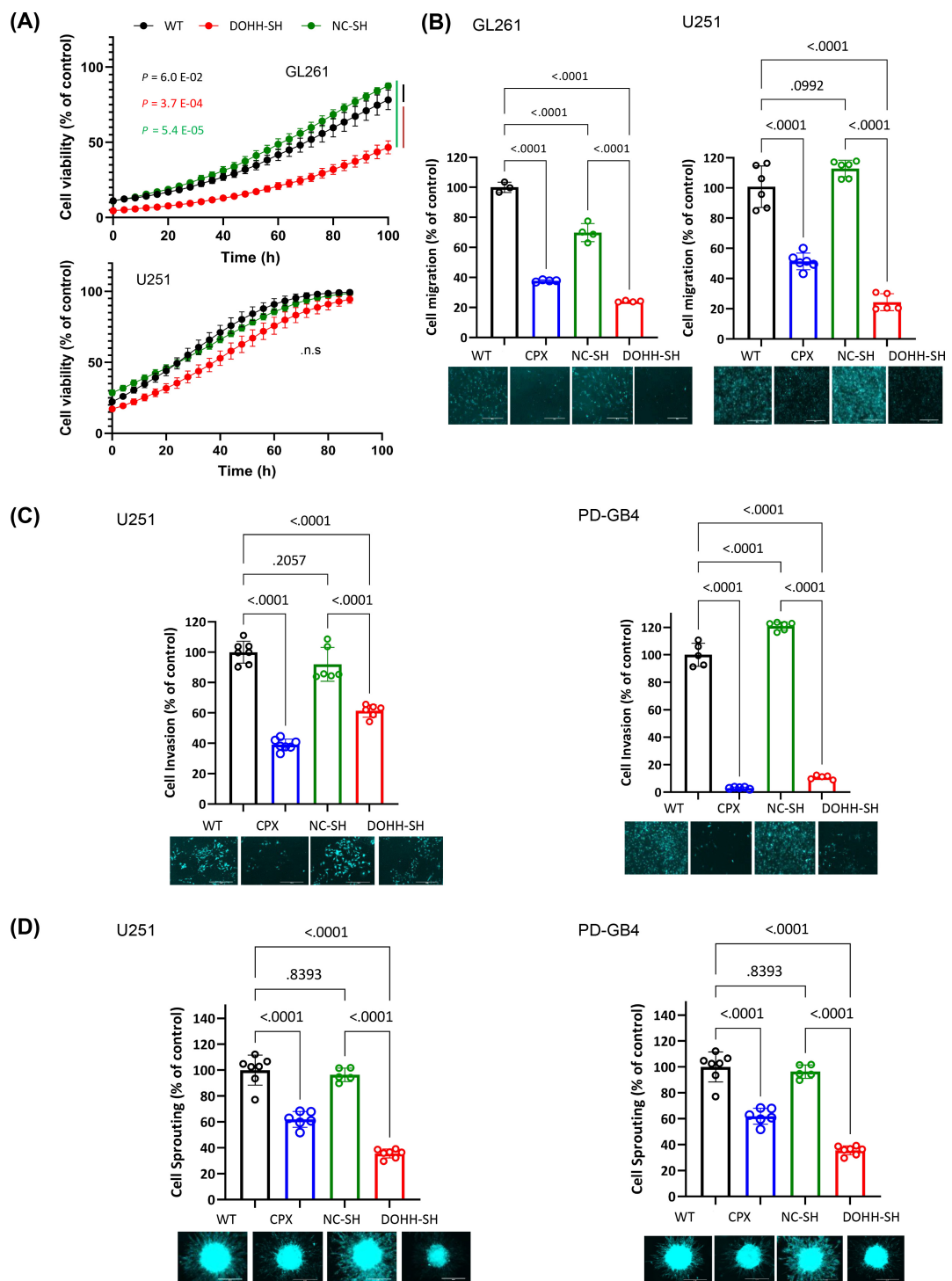


FIGURE 4 DOHH inhibition or silencing decreases proliferation, migration and invasion of GB cells. (A) Proliferation assay of GL261 and U-251 MG GB cells previously infected with DOHH-SH, NC-SH or noninfected, treated with CPX 20 μ M, or left untreated (WT). Significance was determined using an unpaired Student t-test. Data represent mean \pm SD of triplicate wells. Each graph is representative of three biological repeats. (B) Migration assay (8 μ m TransWell) toward fetal bovine serum of iRFP-labeled GL261 and U-251 MG GB cells previously infected with DOHH-SH, NC-SH or noninfected, treated with CPX 20 μ M, or left untreated (WT). Scale bar = 400 μ m. Pictures are representative. Migration was quantitated by ImageJ and plotted in a graph (mean of triplicate wells \pm SD, one representative experiment out of three independent repeats). (C) U-251 MG and PD-GB4GB cell invasion were evaluated by measuring the infiltration through a TransWell coated with Matrigel, toward fetal bovine serum. GB cells were previously infected with DOHH shRNA (DOHH-SH), negative control shRNA (NC-SH) or noninfected, treated with 20 μ M of CPX, or left untreated (WT). Scale bar = 400 μ m. The invasion was quantified by ImageJ and plotted in a graph (mean of triplicate wells \pm SD, one representative experiment out of three independent repeats). (D) Sprouting assay. 3D spheroids comprised of iRFP-labeled, control, DOHH-SH and NC-SH U-251 MG and PD-GB4GB cells, untreated or treated with 20 μ M of CPX were seeded in Matrigel. Sprouting was followed for 48 hours, quantified by ImageJ and plotted in a graph (mean of triplicate wells \pm SD, one representative experiment out of three independent repeats). Scale bar = 400 μ m.

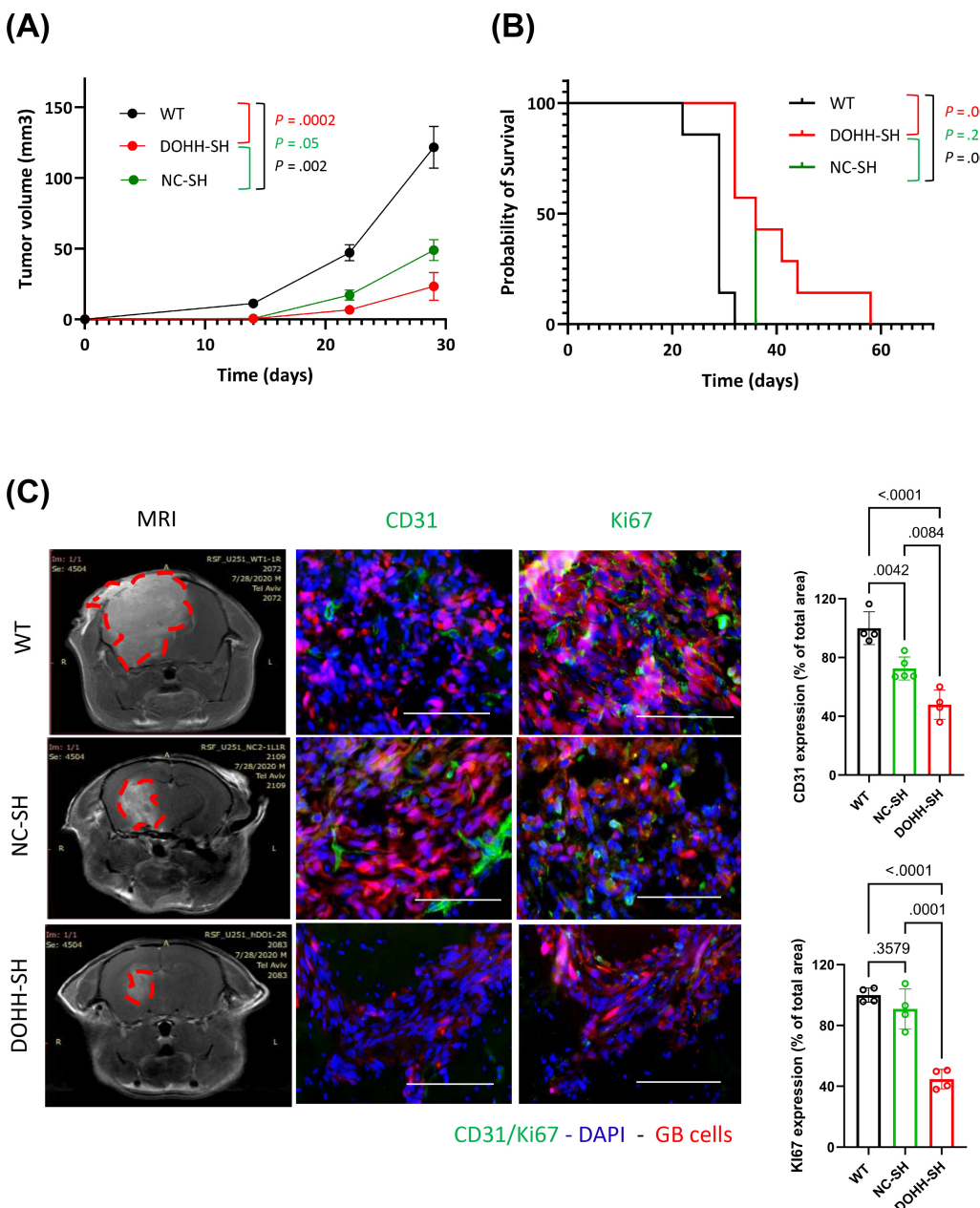


FIGURE 5 DOHH knockdown inhibits tumor growth and prolongs survival in a human GB mouse model. (A) Tumor growth of control (WT), DOHH shRNA (DOHH-SH) and negative control shRNA (NC-SH) U-251 MG human GB in SCID mice was followed by MRI (MR solutions, T1 weighted). Tumor volume was calculated using Radiant software. Data represent mean \pm SEM ($n = 10$ mice per group). Statistical analysis was performed using one-way ANOVA, Dunn's method. (B) Kaplan-Meier curve showing a prolonged survival of DOHH-SH U-251 MG tumor-bearing mice compared to WT ($n = 7$ mice per group). P values were determined using log rank test. (C) Representative MRI and immunostaining images taken on day 29, for blood vessels (CD31) and proliferation (Ki-67). Scale bar = 100 μ m. Immunostaining was quantified using ImageJ software, data shown represent mean \pm SD (3 images per mouse, 3 mice per group).

We found a significant correlation between DOHH and NF- κ B gene signature (including NF- κ B and its master regulators: STAT3, CEBPB and TAZ; Figure 6C). We further evaluated additional routes that drive the mesenchymal phenotype using GEPIA2³⁹ and found a strong correlation between DOHH expression and ADAM17/EGFR activation loop signature (ADAM17, EGFR, GSK3B, AKT1, FOXM1) in GB human samples data from the TCGA (Figure 6D). Activation of the EGFR/AKT/GSK3 β signaling pathway, mediated by FOXM1/

ADAM17 transcriptional activation was previously shown to trigger mesenchymal transition of GB cells.⁴²

Another critical feature of solid tumors that promotes EMT, invasiveness and angiogenesis is hypoxia. HIF-1 α expression profile was found to correlate with the expression levels of N-cadherin, and vimentin.⁴³ Hypoxia induces EMT and leads to the recruitment of myeloid cells, which secrete TGF- β that consequently induces HIF-1 α and promotes glioma progression.⁴⁴⁻⁴⁶ VEGF is one of the main

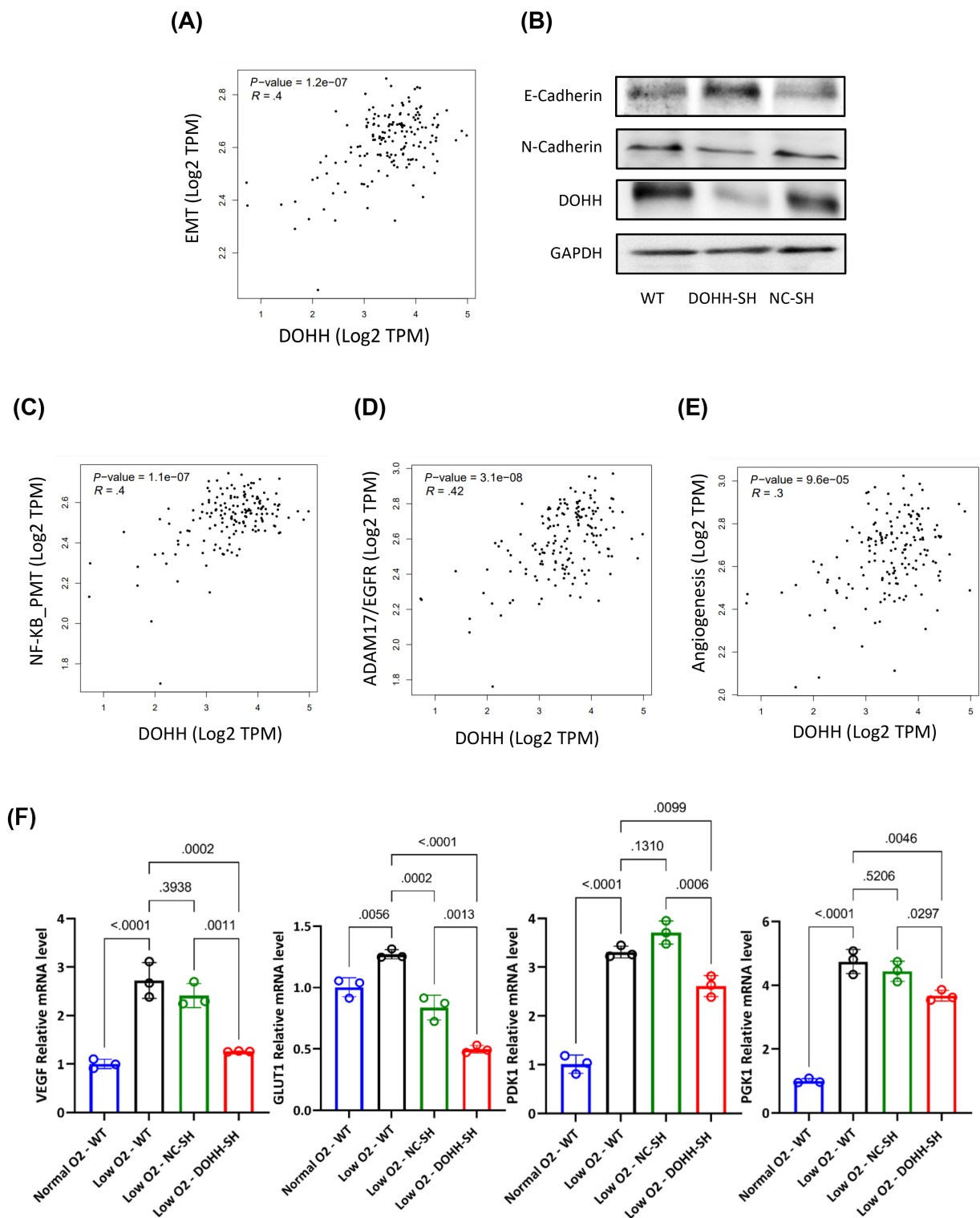


FIGURE 6 DOHH silencing inhibits epithelial to mesenchymal transition (EMT). (A) Correlation between DOHH expression level and EMT gene signature (CDH2, ZEB1, ZEB2, CTNNB, TJP1, VIM, TWIST, Slug and Snail) in human GB samples from the TCGA analyzed by GEPIA2 web server. Data are plotted as log2 TPM (transcripts per million). (B) DOHH silencing upregulates E-cadherin and downregulates N-cadherin, pushing the cells toward a less invasive phenotype. (C) Correlation between DOHH expression level and NF- κ B (nuclear factor kappa-light-chain-enhancer of activated B cells)-driven PMT gene signature (NK- κ B + 3 main master regulators: STAT3, CEBPB, TAZ) in human GB samples (TCGA, GEPIA2). (D) Correlation between DOHH expression level and ADAM17/EGFR gene signature (ADAM17, EGFR, GSK3B, AKT1, FOXM1) in human GB samples (TCGA, GEPIA2). (E) Correlation between DOHH expression level and Angiogenesis gene signature (VEGFR1/2, VEGFA/B, BNIP3, GLUT1, PDK1) in human GB samples (TCGA, GEPIA2). (F) Angiogenesis-related (HIF1-alpha target) genes upregulated following hypoxia are inhibited in DOHH-SH compared to NC-SH and WT U-251 MG GB cells. Real-Time PCR of VEGF, GLUT1, PDK1 and PGK1 genes normalized to GAPDH. Data represent mean \pm SD of triplicate wells. Each graph is representative of three independent repeats.

downstream effectors of HIF-1 α and it plays a critical role in inducing cell migration, proliferation and tube formation. Using GEPIA³⁹ we further found that DOHH expression level significantly correlates with HIF-1 α target genes (angiogenesis-signature) in GB human data from the TCGA (Figure 6E). Moreover, we show that several HIF-1 α target genes, upregulated following hypoxia, are downregulated following silencing of DOHH in human U-251 MG GB cells (Figure 6F).

4 | CONCLUSIONS

In the last few decades, massive progress has been made in our understanding of GB development, genomic patterns and prognostic factors. However, all the new knowledge has resulted in a very limited impact in terms of therapeutic outcome. Identification of diagnostic and prognostic biomarkers is critical to enable the development of novel personalized treatments for GB. Extensive comparative studies between STS and LTS have been challenging due to the scarce availability of LTS tissue samples. Nevertheless, several studies have been performed, underscoring the limitations of existing biomarkers and classification methods in predicting patient prognosis. Although specific gene markers associated with poor survival were discovered, they were linked to small subpopulations, and therapies developed led to only minor benefit within one specific group of patients. Comprehensive proteogenomics analysis of a large cohort of GB human samples led us to some very interesting target proteins, that not much is known about them in the context of GB; like DOHH, which differential expression was associated with survival rate.⁷ DOHH catalyzes the final step of eIF5A hypusination, essential for eIF5A activation and protein synthesis regulation.⁴⁷

Here we show that expression levels of DOHH in human GB inversely correlate with patients' survival. As hypusine is a very selective modification that is also sensitive to pharmacological inhibitors, DOHH represents an attractive therapeutic target for GB.

Using the small molecules CPX and DEF, previously validated as DOHH inhibitors, we achieved reduced proliferation, migration, and invasion of GB cells in vitro. Both compounds are approved for medical use in humans, CPX as a topical antifungal,⁴⁸ and DEF for transfusional iron overload.⁴⁹ Moreover, an oral formulation of CPX showed encouraging results in a phase I clinical trial for hematological malignancies. CPX was well tolerated and achieved improvement in acute myeloid leukemia patients.⁵⁰ Collectively, these findings suggest that both CPX and DEF may be repositioned for systemic use in GB treatment. That of course will require the development of a more suitable formulation that will enable their delivery and accumulation in the brain. We speculate that a combination of DOHH inhibitors with other therapeutic agents could potentially circumvent compensation mechanisms and resistance leading to a synergistic anticancer effect. DOHH knockdown resulted in a similar outcome in all GB cells evaluated, decreasing cell proliferation, migration and invasion, concomitantly with EMT inhibition and downregulation of hypoxia-activated target genes. Silencing DOHH further resulted in tumor growth arrest and prolonged survival in a mouse model of orthotopic human GB, but not in a murine immunocompetent GB mouse model.

A functional connection between the hypusine-polyamine circuit and metastasis-related EMT has been proposed earlier. Silencing and overexpression of eIF5A have previously shown dramatic effects on the expression level of mesenchymal markers such as fibronectin and epithelial markers such as E-cadherin. During EMT, epithelial cells acquire mesenchymal, fibroblast-like properties and display reduced intracellular adhesion and increased motility. EMT depends on a reduction in the expression of cell adhesion molecules, like cadherins that mediate calcium-dependent cell-cell adhesion. E-cadherin is considered an active suppressor of invasion and growth of many epithelial cancers that display up-regulated N-cadherin in addition to the loss of E-cadherin, known as the "cadherin switch".⁵¹ Here, we showed that DOHH silencing inhibits migration, invasion and sprouting of GB cells. Moreover, analysis of TCGA data showed a significant correlation between DOHH expression and EMT signature, which further correlates with HIF-1 α target genes. HIF-1 α target genes, upregulated following hypoxia, are downregulated following the silencing of DOHH in human GB.

In conclusion, we hereby show a proof of principle for a DOHH-based therapy, that can potentially make GB tumors less infiltrative and invasive, leading to patients' longer survival. Small-molecule compounds like CPX and DEF, already approved for clinical use and found safe in human cancer patients can be a great starting point in the development of a repurposed new treatment for GB. We hypothesize that for a heterogeneous and complex disease such as GB, combination with other therapeutic agents, such as P-selectin inhibition,⁵² could potentially circumvent compensation mechanisms and resistance leading to improved efficacy and decreased side effects.

Our findings emphasize the key role that DOHH plays in the regulation of GB aggressiveness, promoting EMT and angiogenesis activation. We further demonstrate the pivotal inhibitory effect of DOHH silencing or inhibition on GB progression in several in vitro and in vivo human and murine models as well as clinical samples.^{53,54}

AUTHOR CONTRIBUTIONS

Paula Ofek: Conceptualization; Experimental; Formal Analysis and Investigation; Writing. **Eilam Yeini:** Experimental; Formal Analysis and Investigation; Writing. **Gali Arad:** Experimental; Formal Analysis and Investigation. **Artem Danilevsky:** Formal Analysis and Investigation. **Sabina Pozzi:** Experimental. **Christian Burgos Luna:** Experimental. **Sahar Israeli Dangoor:** Experimental; Formal Analysis and Investigation. **Rachel Grossman:** Resources. **Zvi Ram:** Resources. **Noam Shomron:** Formal Analysis and Investigation. **Henry Brem:** Resources. **Thomas M. Hyde:** Resources. **Tamar Geiger:** Formal Analysis and Investigation. **Ronit Satchi-Fainaro:** Conceptualization; Formal Analysis and Investigation; Writing; Funding Acquisition; Supervision. All authors reviewed the article and provided comments. The work reported in the article has been performed by the authors unless clearly specified in the text.

ACKNOWLEDGEMENTS

The Satchi-Fainaro laboratory has received partial funding from the European Research Council (ERC) Advanced Grant (835227; 3DBrainStrom); and ERC Proof of Concept (PoC) Grant (862580;

3DCanPredict), The Israel Science Foundation (Grant no. 1969/18); The Israel Cancer Research Fund (PROF-18-682); The Nancy and Peter Brown friends of The Israel Cancer Association (ICA) USA, in memory of Kenny and Michael Adler (20150909); and the Morris Kahn Foundation. P.O. thanks the Naomi Foundation for the Global Research and Training Fellowship in Medical and Life Sciences. The Lieber Institute for Brain Development extends our appreciation to the physicians and staff at the Washington DC, Northern Virginia and State of Maryland Medical Examiners' Offices, as well as the donors and their next of kin for the provision of brain tissue for our study.

CONFLICT OF INTEREST STATEMENT

HB is a consultant for Candel Therapeutics, InSightec, CraniUS, Accelerating Combination Therapies, Catalio Nexus Fund II, LLC, LikeMinds, Inc, Galen Robotics, Inc, Nurami Medical and Intragel and received research funding from NIH, JHU, NICO Myriad Corporation. R.S.-F. is a Board Director at Teva Pharmaceutical Industries Ltd and receives research funding from Merck, all for work unrelated to this article. All other authors have no competing interests to declare.

DATA AVAILABILITY STATEMENT

The MRI data generated in our study were uploaded to the SYNAPSE dataset and can be accessed through the following link: <https://www.synapse.org/#!Synapse:syn36384929/files/>. The proteomics data reported in this article is available in PRIDE: PXD018024.⁵³ The RNA-seq data can be accessed in NCBI's Gene Expression Omnibus⁵⁴ through accession number GEO: GSE149009. The public TCGA dataset is available at <https://www.genome.gov/Funded-Programs-Projects/Cancer-Genome-Atlas>. Correlation analyses between DOHH expression and EMT/NF-kB-driven/ADAM17/EGFR gene signatures (see legend of Figure 6C-E) were based on GEPIA2 public dataset (<http://gepia2.cancer-pku.cn/#correlation>), from which GBM tumor expression dataset was selected and Pearson correlation was applied. We have previously published the proteomics and RNA-seq data and only one of the found targets, DOHH, was studied in the current article. Further information is available from the corresponding author upon request.

ETHICS STATEMENT

All animal experiments were performed under approval by the Animal Care and Use Committee (IAUC) of Tel Aviv University, in accordance with NIH guidelines (approval no. 01-19-015, 01-19-097). Experiments involving human GB tissues were performed with the approval of the Institutional Review Board (IRB) committee of Tel Aviv Sourasky Medical Center and in compliance with all legal and ethical considerations for human subject research (approval no. 0735-13-TLV). Healthy human brain tissues: Post-mortem human brain tissue was obtained by autopsy from the Offices of the Chief Medical Examiner of the District of Columbia and of the Commonwealth of Virginia, Northern District, all with informed consent from the legal next of kin (protocol 90-M-0142 approved by the NIMH/NIH IRB). Additional post-mortem human brain tissue samples were provided by the National Institute of Child Health and Human Development Brain and Tissue Bank for Developmental

Disorders (<http://www.BTBANK.org>) under contracts NO1-HD-4-3368 and NO1-HD-4-3383. The IRB of the University of Maryland at Baltimore and the State of Maryland approved the protocol and the tissue was donated to the Lieber Institute for Brain Development under the terms of a Material Transfer Agreement.

ORCID

Paula Ofek  <https://orcid.org/0000-0002-8516-1107>

Elam Yeini  <https://orcid.org/0000-0003-3491-3994>

Ronit Satchi-Fainaro  <https://orcid.org/0000-0002-7360-7837>

TWITTER

Ronit Satchi-Fainaro  @RSFLab

REFERENCES

1. Wong ET, Lok E, Swanson KD. Alternating electric fields therapy for malignant gliomas: from bench observation to clinical reality. *Prog Neurol Surg*. 2018;32:180-195.
2. Lacroix M, Abi-Said D, Fourney DR, et al. A multivariate analysis of 416 patients with glioblastoma multiforme: prognosis, extent of resection, and survival. *J Neurosurg*. 2001;95:190-198.
3. Burgenske DM, Yang J, Decker PA, et al. Molecular profiling of long-term IDH-wildtype glioblastoma survivors. *Neuro Oncol*. 2019;21:1458-1469.
4. Verhaak RG, Hoadley KA, Purdom E, et al. Integrated genomic analysis identifies clinically relevant subtypes of glioblastoma characterized by abnormalities in PDGFRA, IDH1, EGFR, and NF1. *Cancer Cell*. 2010;17:98-110.
5. Gautam P, Nair SC, Gupta MK, et al. Proteins with altered levels in plasma from glioblastoma patients as revealed by iTRAQ-based quantitative proteomic analysis. *PLoS One*. 2012;7:e46153.
6. Kumar DM, Thota B, Shinde SV, et al. Proteomic identification of haptoglobin alpha2 as a glioblastoma serum biomarker: implications in cancer cell migration and tumor growth. *J Proteome Res*. 2010;9: 5557-5567.
7. Yanovich-Arad G, Ofek P, Yeini E, et al. Proteogenomics of glioblastoma associates molecular patterns with survival. *Cell Rep*. 2021;34: 108787.
8. Savulescu J. Thalassaemia major: the murky story of deferiprone. *BMJ*. 2004;328:358-359.
9. Epis MR, Giles KM, Candy PA, Webster RJ, Leedman PJ. miR-331-3p regulates expression of neuropilin-2 in glioblastoma. *J Neurooncol*. 2014;116:67-75.
10. Preukschas M, Hagel C, Schulte A, et al. Expression of eukaryotic initiation factor 5A and hypusine forming enzymes in glioblastoma patient samples: implications for new targeted therapies. *PLoS One*. 2012;7:e43468.
11. Hanauske-Abel HM, Park MH, Hanaukske AR, Popowicz AM, Lalande M, Folk JE. Inhibition of the G1-S transition of the cell cycle by inhibitors of deoxyhypusine hydroxylation. *Biochim Biophys Acta*. 1994;1221:115-124.
12. Park MH, Wolff EC, Lee YB, Folk JE. Antiproliferative effects of inhibitors of deoxyhypusine synthase. Inhibition of growth of Chinese hamster ovary cells by guanyl diamines. *J Biol Chem*. 1994;269: 27827-27832.
13. Sievert H, Pallmann N, Miller KK, et al. A novel mouse model for inhibition of DOHH-mediated hypusine modification reveals a crucial function in embryonic development, proliferation and oncogenic transformation. *Dis Model Mech*. 2014;7:963-976.
14. Eberhard Y, McDermott SP, Wang X, et al. Chelation of intracellular iron with the antifungal agent ciclopirox olamine induces cell death in leukemia and myeloma cells. *Blood*. 2009;114:3064-3073.

15. Luo Y, Zhou H, Liu L, et al. The fungicide ciclopirox inhibits lymphatic endothelial cell tube formation by suppressing VEGFR-3-mediated ERK signaling pathway. *Oncogene*. 2011;30:2098-2107.
16. Zhou H, Shen T, Luo Y, et al. The antitumor activity of the fungicide ciclopirox. *Int J Cancer*. 2010;127:2467-2477.
17. Fujimura K, Wright T, Strnadel J, et al. A hypusine-eIF5A-PEAK1 switch regulates the pathogenesis of pancreatic cancer. *Cancer Res*. 2014;74:6671-6681.
18. Clement PM, Hanauske-Abel HM, Wolff EC, Kleinman HK, Park MH. The antifungal drug ciclopirox inhibits deoxyhypusine and proline hydroxylation, endothelial cell growth and angiogenesis in vitro. *Int J Cancer*. 2002;100:491-498.
19. Kim Y, Schmidt M, Endo T, Lu D, Carson D, Schmidt-Wolf IG. Targeting the Wnt/beta-catenin pathway with the antifungal agent ciclopirox olamine in a murine myeloma model. *In Vivo*. 2011;25: 887-893.
20. Gupta AK. Ciclopirox: an overview. *Int J Dermatol*. 2001;40:305-310.
21. Simoes RV, Veeraperumal S, Serganova IS, et al. Inhibition of prostate cancer proliferation by Deferiprone. *NMR Biomed*. 2017;30:e3712.
22. Fiorillo M, Toth F, Brindisi M, Sotgia F, Lisanti MP. Deferiprone (DFP) targets cancer stem cell (CSC) propagation by inhibiting mitochondrial metabolism and inducing ROS production. *Cell*. 2020;9(6):1529.
23. Epis MR, Giles KM, Kalinowski FC, Barker A, Cohen RJ, Leedman PJ. Regulation of expression of deoxyhypusine hydroxylase (DOHH), the enzyme that catalyzes the activation of eIF5A, by miR-331-3p and miR-642-5p in prostate cancer cells. *J Biol Chem*. 2012;287:35251-35259.
24. Anders S, Pyl PT, Huber W. HTSeq—a python framework to work with high-throughput sequencing data. *Bioinformatics*. 2015;31:166-169.
25. Santana-Magal N. Melanoma-secreted lysosomes trigger monocyte-derived dendritic cell apoptosis and limit cancer immunotherapy. *Cancer Res*. 2020;80:1942-1956.
26. Ferber S, Tiram G. Co-targeting the tumor endothelium and P-selectin-expressing glioblastoma cells leads to a remarkable therapeutic outcome. *Elife*. 2017;6:e25281.
27. Cox J, Mann M. 1D and 2D annotation enrichment: a statistical method integrating quantitative proteomics with complementary high-throughput data. *BMC Bioinform*. 2012;13(Suppl 16):S12.
28. Everaert C, Luypaert M, Maag JLV, et al. Benchmarking of RNA-sequencing analysis workflows using whole-transcriptome RT-qPCR expression data. *Sci Rep*. 2017;7:1559.
29. Memin E, Hoque M, Jain MR, et al. Blocking eIF5A modification in cervical cancer cells alters the expression of cancer-related genes and suppresses cell proliferation. *Cancer Res*. 2014;74:552-562.
30. Tao C, Huang K, Shi J, Hu Q, Li K, Zhu X. Genomics and prognosis analysis of epithelial-mesenchymal transition in glioma. *Front Oncol*. 2020;10(183).
31. Puleston DJ, Baixauli F, Sanin DE, et al. Polyamine metabolism is a central determinant of helper T cell lineage fidelity. *Cell*. 2021;184: 4186-4202.
32. Chin A, Bieberich CJ, Stewart TM, Casero RA. Polyamine depletion strategies in cancer: remodeling the tumor immune microenvironment to enhance anti-tumor responses. *Med Sci*. 2022;10:31.
33. Huang Z, Huang S. Reposition of the fungicide ciclopirox for cancer treatment. *Recent Pat Anticancer Drug Discov*. 2021;16:122-135.
34. Weir SJ, Dandawate P, Standing D, et al. Fosciclopirox suppresses growth of high-grade urothelial cancer by targeting the gamma-secretase complex. *Cell Death Dis*. 2021;12:562.
35. Al-Zubaydi F, Gao D, Kakkar D, et al. Breast intraductal nanoformulations for treating ductal carcinoma in situ II: dose de-escalation using a slow releasing/slow bioconverting prodrug strategy. *Drug Deliv Transl Res*. 2022;12:240-256.
36. Balabanov S, Gontarewicz A, Ziegler P, et al. Hypusination of eukaryotic initiation factor 5A (eIF5A): a novel therapeutic target in BCR-ABL-positive leukemias identified by a proteomics approach. *Blood*. 2007;109:1701-1711.
37. Yin J, Che G, Jiang K, et al. Ciclopirox olamine exerts tumor-suppressor effects via topoisomerase II alpha in lung adenocarcinoma. *Front Oncol*. 2022;12:791916.
38. Wang FW, Guan XY, Xie D. Roles of eukaryotic initiation factor 5A2 in human cancer. *Int J Biol Sci*. 2013;9:1013-1020.
39. Tang Z, Kang B, Li C, Chen T, Zhang Z. GEPIA2: an enhanced web server for large-scale expression profiling and interactive analysis. *Nucleic Acids Res*. 2019;47:W556-W560.
40. Huber MA, Azoitei N, Baumann B, et al. NF-kappaB is essential for epithelial-mesenchymal transition and metastasis in a model of breast cancer progression. *J Clin Invest*. 2004;114:569-581.
41. Bhat KPL, Balasubramanyan V, Vaillant B, et al. Mesenchymal differentiation mediated by NF-kappaB promotes radiation resistance in glioblastoma. *Cancer Cell*. 2013;24:331-346.
42. Zhang C, Han X, Xu X, et al. FoxM1 drives ADAM17/EGFR activation loop to promote mesenchymal transition in glioblastoma. *Cell Death Dis*. 2018;9:469.
43. Lai K, Luo C, Zhang X, et al. Regulation of angiogenin expression and epithelial-mesenchymal transition by HIF-1alpha signaling in hypoxic retinal pigment epithelial cells. *Biochim Biophys Acta*. 1862;2016: 1594-1607.
44. Heddleston JM, Li Z, McLendon RE, Hjelmeland AB, Rich JN. The hypoxic microenvironment maintains glioblastoma stem cells and promotes reprogramming towards a cancer stem cell phenotype. *Cell Cycle*. 2009;8:3274-3284.
45. Bar EE, Lin A, Mahairaki V, Matsui W, Eberhart CG. Hypoxia increases the expression of stem-cell markers and promotes clonogenicity in glioblastoma neurospheres. *Am J Pathol*. 2010;177:1491-1502.
46. Evans SM, Judy KD, Dunphy I, et al. Hypoxia is important in the biology and aggression of human glial brain tumors. *Clin Cancer Res*. 2004;10:8177-8184.
47. Park MH, Wolff EC. Hypusine, a polyamine-derived amino acid critical for eukaryotic translation. *J Biol Chem*. 2018;293:18710-18718.
48. Subissi A, Monti D, Togni G, Maillard F. Ciclopirox: recent nonclinical and clinical data relevant to its use as a topical antimycotic agent. *Drugs*. 2010;70:2133-2152.
49. Neufeld EJ. Update on iron chelators in thalassemia. *Hematology Am Soc Hematol Educ Program*. 2010;2010:451-455.
50. Minden MD, Hogge DE, Weir SJ, et al. Oral ciclopirox olamine displays biological activity in a phase I study in patients with advanced hematologic malignancies. *Am J Hematol*. 2014;89:363-368.
51. Loh CY, Chai JY, Tang TF, et al. The E-cadherin and N-cadherin switch in epithelial-to-mesenchymal transition: signaling, therapeutic implications, and challenges. *Cell*. 2019;8(10):1118.
52. Yeini E, Ofek P, Pozzi S, et al. P-selectin axis plays a key role in microglia immunophenotype and glioblastoma progression. *Nat Commun*. 2021;12:1912.
53. Perez-Riverol Y, Moreno P. Scalable data analysis in proteomics and metabolomics using BioContainers and workflows engines. *Proteomics*. 2020;20:e1900147.
54. Edgar R, Domrachev M, Lash AE. Gene expression omnibus: NCBI gene expression and hybridization array data repository. *Nucleic Acids Res*. 2002;30:207-210.

SUPPORTING INFORMATION

Additional supporting information can be found online in the Supporting Information section at the end of this article.

How to cite this article: Ofek P, Yeini E, Arad G, et al.

Deoxyhypusine hydroxylase: A novel therapeutic target differentially expressed in short-term vs long-term survivors of glioblastoma. *Int J Cancer*. 2023;153(3):654-668. doi:10.1002/ijc.34545